materials

MDPI

Article

Transformation Behavior of Fe, V and Ti in Pre–Reduced Vanadium–Titanium Magnetite During Electric Furnace Smelting

Conglin Yao [1], Baolin Tan [2], Bing Hu [1], Fuqiang Zheng [1], Yong Yu [2,*] and Pengbo Wang [3,*]

[1] Zhongye Changtian International Engineering Co., Ltd., Changsha 410205, China
[2] Engineering Research Center of Metallurgical Energy Conservation and Emission Reduction, Ministry of Education, School of Metallurgical and Energy Engineering, Kunming University of Science and Technology, Kunming 650093, China
[3] Department of Industrial and Systems Engineering, The Hong Kong Polytechnic University, Hong Kong, China
* Correspondence: 20230010@kust.edu.cn (Y.Y.); 21039441r@connect.polyu.hk (P.W.); Tel.: +86–185–8934–5101 (Y.Y.); +86–186–5566–5283 (P.W.)

Highlights

- The migrations of Fe, V and Ti during reduction smelting were clarified.
- The recovery ratios of V, Fe and Ti reached 94.56%, 99.61% and 98.87%.
- This paper has significant implications for pre–reduced vanadium–titanium magnetite smelting.

Abstract

Vanadium–titanium magnetite is an important global strategic resource, with proven reserves exceeding 40 billion tons. Currently, the direct reduction–electric furnace route is regarded as the most promising process for VTM treatment. However, the transformation mechanisms of Fe, V and Ti remain insufficiently understood, constraining industrial implementation. In this study, the transformations of Fe, V and Ti during reduction smelting were systematically clarified, and the effects of MgO, CaO and semi–coke were evaluated. MgO addition promoted the formation of $MgAl_2O_4$, $(Ti,V)_2O_3$ and $(Mg,V)_xTi_{3-x}O_5$, hindering slag–alloy separation. In contrast, with CaO as a modifier, $FeTiO_3$ in the raw material was reduced by C to yield Fe and $V_xTi_{3-x}O_5$, which was further reduced to $(Ti,V)_2O_3$. The added CaO reacted with $(Ti,V)_2O_3$ to generate $CaTiO_3$ and (V_xO_y), chemically dissolved V. Concurrently, CaO reacted with silicates to produce $CaAl_2Si_2O_8$, facilitating the sedimentation of the Fe–V alloy. Under the optimal conditions of 1873 K, a holding time of 20 min and additions of 2.5 wt% semi–coke and 12 wt% CaO, the recoveries of V, Fe and Ti reached 94.56%, 99.61% and 98.87%. In comparison, conventional processes typically achieved Fe and V recoveries of only approximately 90% and 70%. These findings support the industrial application of pre–reduced VTM.

Keywords: vanadium–titanium magnetite; transformation mechanisms of Fe; V and Ti; direct reduction–electric furnace process; efficient resource utilization

Check for updates

Academic Editor: Jiangshan Zhang

Received: 6 August 2026
Revised: 30 September 2026
Accepted: 16 October 2026
Published: 29 October 2026

Copyright: © 2026 by the authors. Licensee MDPI, Basel, Switzerland. This article is an open access article distributed under the terms and conditions of the Creative Commons Attribution (CC BY) license.

1. Introduction

Vanadium (V) and titanium (Ti) are globally important strategic metals recognized by China, the United States and the European Union [1–3]. V and Ti are mainly hosted

in vanadium–titanium magnetite (VTM) [4–6]. VTM is characterized by abundant reserves and wide global distribution, with proven reserves exceeding 40 billion tons [7]. It typically contains 11–58 wt% Fe, 11–21 wt% TiO_2 and 0.2–1.9 wt% V_2O_5 [3,8–10]. Mineralogically, VTM is composed mainly of titanomagnetite, ilmenite, sulfides and gangue minerals, with gangue phases primarily consisting of sphene, chlorite, pyroxene and plagioclase. Owing to its distinctive mineralogical structure, efficient utilization of VTM remains highly challenging.

The blast furnace–converter smelting route is the principal process used for VTM treatment in China [11,12]. This route has been widely adopted because of its high maturity and large–scale production capacity. In this process, sintered VTM pellets and coke are charged into a blast furnace for high–temperature smelting at 1723–1823 K, where selective reduction and separation occur. During this stage, V is transferred to the Fe liquid phase, whereas Ti accumulates in the blast furnace slag [13–15]. The V–bearing hot metal is subsequently sent to the converter for blowing, where V is separated from the Fe liquid phase by oxidation and transferred to the slag. Finally, V is extracted from the slag via leaching [16]. However, the V recovery is only approximately 47%, which is unsatisfactory. Meanwhile, a large amount of blast furnace slag containing 22% TiO_2 remains underutilized, resulting in concerns regarding resource waste. Compared with the blast furnace–converter route, the non–blast furnace smelting process for VTM has attracted increasing attention because of its potential advantages, including a shorter process flow, lower carbon emissions and higher recoveries of V and Ti. The direct reduction–electric furnace route has become a mainstream non–blast furnace process [17,18]. In this process, VTM is first pre–reduced at 1273–1373 K, during which Fe is converted to metallic iron, while Ti remains in the slag phase, to achieve the preliminary separation of Fe and Ti. The pre–reduced VTM is subjected to smelting reduction in an electric furnace to produce an Fe–V alloy and Ti–rich slag, for which the recoveries of Fe and V are 90% and 70%, respectively [19]. Approximately 80% of Ti can be extracted from Ti–rich slag through acid leaching. Nevertheless, owing to the complex mineral structure of pre–reduced VTM and the unclear transformation mechanisms of Fe, V and Ti, improvement in the recoveries of Fe, V and Ti remains difficult.

To improve the utilization efficiency of pre–reduced VTM, numerous studies have been conducted [19–22]. Zhang et al. achieved recoveries of 93.67% for Fe, 72.68% for V and 99.72% for Ti at 1473 K for 2 h, a bed thickness of 42.5 mm, a C/O molar ratio of 1.7 and the addition of 70 wt% Na_2CO_3 [19]. In this process, Fe oxides were reduced to metallic Fe and separated from the slag for recovery, while V was converted to water–soluble sodium vanadate. Subsequently, the slag was separated into V leachate and Ti slag via water leaching. In addition, Chen et al. reported that acid oxides in VTM could be destroyed by Na_2CO_3 to generate a Na–rich melt, thereby reducing slag viscosity and accelerating the reaction rate [20]. Yang et al. first pelletized a mixture of VTM with 5% coke and 3% bentonite, followed by reduction smelting at 1773 K for 30 min [21]. In that study, the total coke dosage was fixed at 15%, the basicity was adjusted by adding CaO and SiO_2, controlled at 1.2, and an appropriate amount of CaF_2 was introduced to regulate slag fluidity. Under the optimized conditions, efficient separation of the Fe–V alloy and Ti–rich slag was achieved, with recoveries of 99.86% for Fe, 95.64% for V and 93.54% for Ti. However, due to the high coke dosage of 15%, this process generates substantial CO and CO_2 emissions during production. This may result in a significant carbon footprint. Although CaF_2 is added as a flux to improve slag fluidity, its application may introduce a risk of F pollution and thus pose potential environmental hazards, making it inconsistent with the development trend of green metallurgy [22–24].

Furthermore, the effects of CaO and MgO additions on VTM reduction and smelting have been widely investigated. Regarding CaO addition, Cheng et al. studied the effect

of calcium oxide on the crushing strength, reduction, and smelting performance of high–chromium VTM pellets [25], and Wang et al. optimized the basicity of high–Ti slag for efficient smelting of VTM metallized pellets [26]. With respect to MgO addition, Chen et al. investigated the feasibility of preparing magnesium titanate via carbothermic reduction of VTM concentrates [27] and the effects of MgO on the reduction of VTM concentrates with char [28]. Gao et al. also reported the property variations of low–grade VTM pellets with different MgO contents [29]. These studies provide valuable insights into the roles of CaO and MgO in the reduction and smelting of VTM. However, the specific migration and distribution mechanisms of Fe, V, and Ti during the electric furnace reduction smelting of pre–reduced VTM under different modifier and reductant dosages remain to be systematically clarified. Building on these studies, the present study proposes a novel smelting strategy involving VTM, CaO, MgO and semi–coke to achieve more efficient resource utilization. The objective is to clarify the transformation behavior of Fe, V and Ti and to evaluate the effects of CaO, MgO, semi–coke dosage and cooling rate, thereby supporting the industrial application of pre–reduced VTM.

Building on these studies, the present study proposed a novel smelting strategy involving VTM, CaO, MgO and semi–coke to achieve more efficient resource utilization. CaO and MgO were introduced as modifiers to release chemically dissolved V and lower the melting point of VTM. Using this strategy, Fe and V were effectively enriched in the Fe–V alloy, whereas Ti was retained in the slag. The effects of CaO, MgO and semi–coke dosage were systematically evaluated and the transformation mechanisms of Fe, V and Ti during smelting were elucidated.

2. Materials and Methods

The pre–reduced VTM was obtained from a smelter in Changsha, China, composed of 57.74 wt% Fe, 1.73 wt% V_2O_5 and 8.81 wt% TiO_2 (Table 1). The XRD pattern (phase analysis; Rigaku, Tokyo, Japan, TTR–Type III diffractometer) shown in Figure 1 identified Fe, $FeTiO_3$ and Fe_3O_4 as the principal phases, whereas V was not detected because its content was too low for XRD analysis. As further revealed by the electron probe microanalysis (EPMA; JEOL, Tokyo, Japan, JXA–8230) results in Figure 2, V was mainly distributed in the FeTiO3 phase, with a measured content of 1.40 wt%. In the conventional blast furnace–converter route, Fe and V are transferred into the molten iron phase and Ti is retained in the slag and separated based on the density difference between the two phases. Semi–coke was supplied by a smelter in Yunnan, China, with 80.03 wt% fixed carbon (Table 2).

Table 1. The chemical analysis of the pre–reduced VTM/wt%.

Element	T Fe	Fe	V_2O_5	TiO_2	SiO_2	MgO	Al_2O_3
Content	57.74	44.21	1.73	8.81	3.18	1.36	4.84

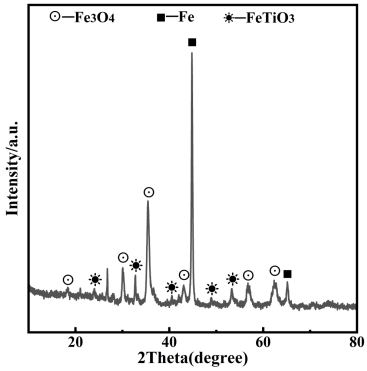


Figure 1. XRD pattern of the pre–reduced VTM.

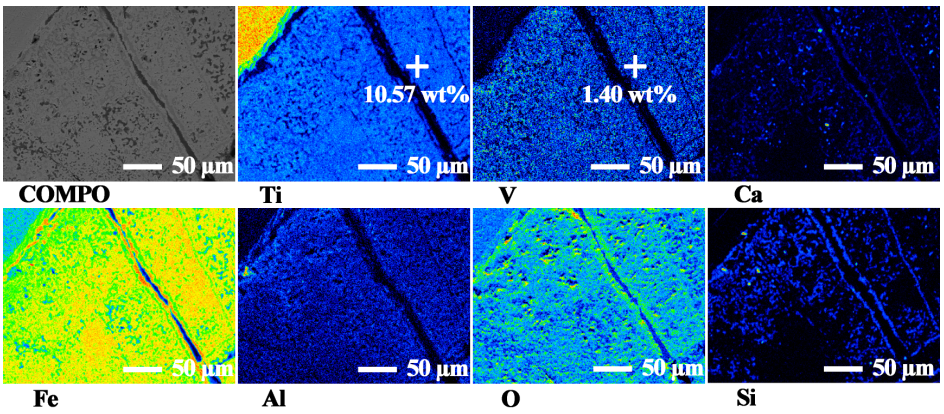


Figure 2. EPMA analysis of the pre–reduced VTM.

Table 2. Semi–coke proximate analysis (wt%).

Fixed Carbon	Ash	Volatile Matter
80.03	9.40	10.57

2.1. Methods

2.1.1. Experimental Methods

The experimental procedure is illustrated in Figure 3. Dried pre–reduced VTM powder (<75 μm), modifier (MgO or CaO) and semi–coke were blended at different mass ratios. Subsequently, 5–8 wt% water was added for pelletizing to produce pellets with a diameter of 1 cm, followed by drying at 378 K for 2 h. The additions of semi–coke and MgO/CaO were varied within the ranges of 1.5–4.5 wt% and 3–15 wt%, respectively. The prepared mixtures (approximately 100 g, 70–90 pieces) in an alumina crucible (inner radius: 30 mm; height: 100 mm) were then charged into a precision–controlled atmosphere furnace (Model: STQ–12–17, Henan Sante Furnace Technology Co., Ltd., Luoyang, China) and heated at 1873 K for 20 min under a flowing high–purity Ar atmosphere (99.90%, 200 mL/min). The furnace has internal chamber dimensions of 200 mm × 300 mm × 200 mm and a temperature control accuracy of ±1 K. The furnace is gas–tight and operates under a flowing high–purity Ar atmosphere (99.90%, 200 mL/min). A U–type thermocouple is positioned in the constant–temperature zone close to the crucible and is connected to a PID controller for temperature control. After smelting, the samples were cooled naturally to 298 K inside the furnace. The cooling occurred from approximately 1873 K to 1273 K in about 50 min, corresponding to an average cooling rate of about 12 K/min, and from 1273 K to 323 K in about 5 h.

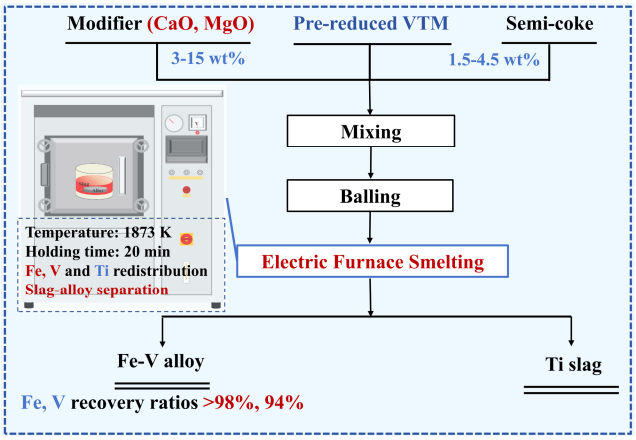


Figure 3. Detailed experimental procedure.

2.1.2. The Formulas and Methods

The recovery of Fe and V into the metal phase was calculated by:

$$\text{Recovery}_{Fe,V}\ (\%) = [1 - (m_{slag,after} \times w_{Fe,V,slag,after})/(m_{feed} \times w_{Fe,V,feed})] \times 100\%$$

where $m_{slag,after}$ is the mass of the slag after smelting, $w_{Fe,V,slag,after}$ is the mass fraction of Fe or V in the slag after smelting, m_{feed} is the total mass of the feed (pre–reduced VTM + modifiers + reductant), and $w_{Fe,V,feed}$ is the mass fraction of Fe or V in the feed.

The recovery of Ti into the slag phase was calculated by:

$$\text{Recovery}_{Ti}\ (\%) = (m_{slag,after} \times w_{Ti,slag,after})/(m_{feed} \times w_{Ti,feed})] \times 100\%$$

where $w_{Ti,slag,after}$ is the mass fraction of Ti in the alloy after smelting and $w_{Ti,feed}$ is the mass fraction of Ti in the feed.

2.1.3. Characterization

To ensure analytical reliability, chemical compositions were determined using the standard chemical methods GB/T14506.32–2019 [30] and GB/T14353.1–2010 [31], along with inductively coupled plasma optical emission spectrometry (ICP–OES, YB/T 4177.2–2025) [32]. Each sample was measured in triplicate, and the reported values represent the average of the three measurements. Phase identification was achieved by X–ray diffraction (XRD) using a RIGAKU TTRIII–18KW diffractometer (Rigaku, Tokyo, Japan) operated at 40 kV and 40 mA with Cu–Kα radiation. The scans were collected over 10–90° at a scanning rate of 10°/min and a step size of 0.02°. Moreover, EPMA coupled with energy–dispersive X–ray spectroscopy (EDS, JEOL, Tokyo, Japan, JXA–8230) was employed to characterize the phase evolution and elemental distribution in the samples under operating conditions of 10–25 kV and 2–50 nA.

3. Thermodynamic Analysis

3.1. Carbothermal Reduction Smelting of Pre–Reduced VTM

Multiphase equilibrium calculations based on the process mineralogy of pre–reduced VTM (FactSage 8.1 Equilib module; Tables 3 and 4, and Figure 4) indicated that at a C addition of 2 wt%, the equilibrium products were dominated by the Fe_{liq} phase and slag. Temperature appears to slightly affect the distribution of V and C, and strongly affect viscosity. More than 90% of Fe was distributed in the Fe_{liq} phase, with an Fe grade exceeding 99 wt% (Table 5). In comparison, the V recovery improved only slightly, increasing from 0.24 to 0.66% as the temperature increased, while the slag still contained more than 4 wt% V (Table 6), indicating poor V recoverability. On the other hand, Ti was completely recovered over 1673–1873 K, and its concentration in the slag increased to 19.72 wt% Ti (Table 6). Additionally, the slag viscosity decreased markedly from 0.100 to 0.064 Pa·s with increasing temperature (FactSage Viscosity module; Tables 4–7).

As shown in Figure 5, when 6 wt% C was added at 1673 K, 81% of V was transferred to the Fe_{liq} phase, leaving only 0.30% of V in the slag. When the temperature was further increased to 1873 K, the fraction of V distributed in the Fe_{liq} phase decreased to 89.3%, whereas the V content in the slag increased to 0.75%. Throughout the investigated temperature range, more than 89% of V entered the Fe_{liq} phase, along with 18% of Ti. These results indicate that increasing the C dosage enabled the simultaneous and efficient recovery of Fe, V and Ti, exceeding 99%, 89% and 82%, respectively. The Fe_{liq} phase contained 94 wt% Fe and 1.2 wt% V (Table 8), whereas the impurity levels of Si and C remained low. Meanwhile, the Ti content in the slag phase increased to more than 32% (Table 9). However, the reduction of (FeO) in the slag caused a pronounced increase in the slag

viscosity with increasing temperature (Tables 7–10), which severely hindered mass transfer and slag–metal separation. The slag system must be optimized.

Table 3. Phases/species assumed and state modeling assumptions used in the multiphase equilibrium calculations.

Input Phases	Fe	Fe_3O_4	V	$FeTiO_3$	SiO_2	MgO	Al_2O_3	CaO	C
Quality	44.21	10.17	0.97	16.73	3.18	1.36	4.84	0.15	<A>
Temperature	1673 K–1873 K								
Databases	FToxid			FTmisc				FactPS	
Compound species	Ideal Gas			Pure liquids				Pure solids	
Solution phase	Fe–liq			A–Slag–liq all oxides + S				A–Spinel	

Table 4. Components assumed in the slag viscosity calculation.

Input Phases	SiO_2	Al_2O_3	TiO_2	MgO	CaO
Databases	Glasses				
Temperature	1673 K–1873 K				

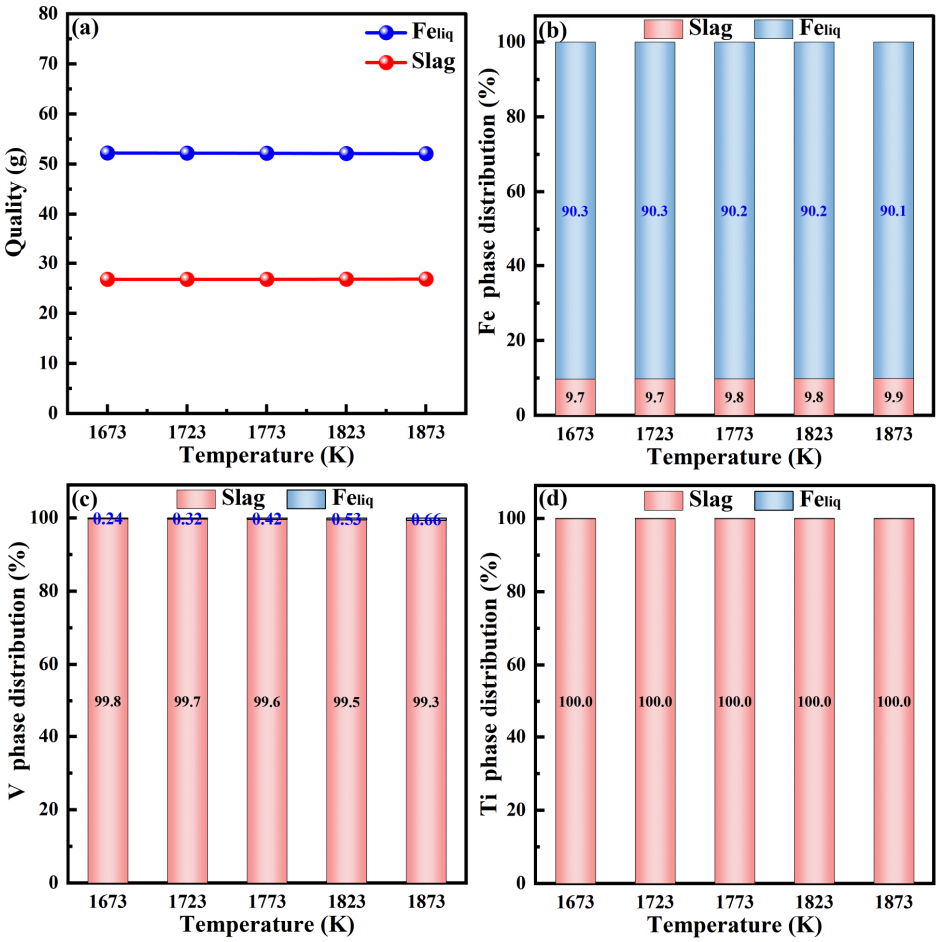


Figure 4. Calculated effect of temperature on the multicomponent complex thermodynamics during smelting with 2 wt% C addition: (**a**) phase distribution; (**b**) distribution behavior of Fe phases; (**c**) distribution behavior of V phases; (**d**) distribution behavior of Ti phases.

Table 5. Calculated composition of the liquid Fe phase with 2 wt% C addition (wt%).

Temperature/K	Fe	V	Si	Al	C
1673	99.877	0.004	0.000	0.000	0.102
1723	99.892	0.006	0.000	0.000	0.080
1773	99.900	0.008	0.001	0.000	0.064
1823	99.903	0.010	0.001	0.000	0.052
1873	99.900	0.012	0.002	0.000	0.042

Table 6. Calculated slag composition with 2 wt% C addition (wt%).

Temperature/K	Fe	V	Ti	Ca	Si	Al	Mg	O
1673	20.89	3.62	19.72	0.40	5.55	9.57	3.06	37.19
1723	20.95	3.61	19.72	0.40	5.55	9.57	3.06	37.13
1773	21.05	3.61	19.71	0.40	5.55	9.56	3.06	37.07
1823	21.16	3.60	19.69	0.40	5.54	9.55	3.06	37.00
1873	21.28	3.59	19.67	0.40	5.53	9.54	3.06	36.93

Table 7. Calculated slag viscosity as a function of temperature with 2 wt% C addition.

Temperature/K	Viscosity/Pa·s
1673	0.100
1723	0.081
1773	0.066
1823	0.055
1873	0.046

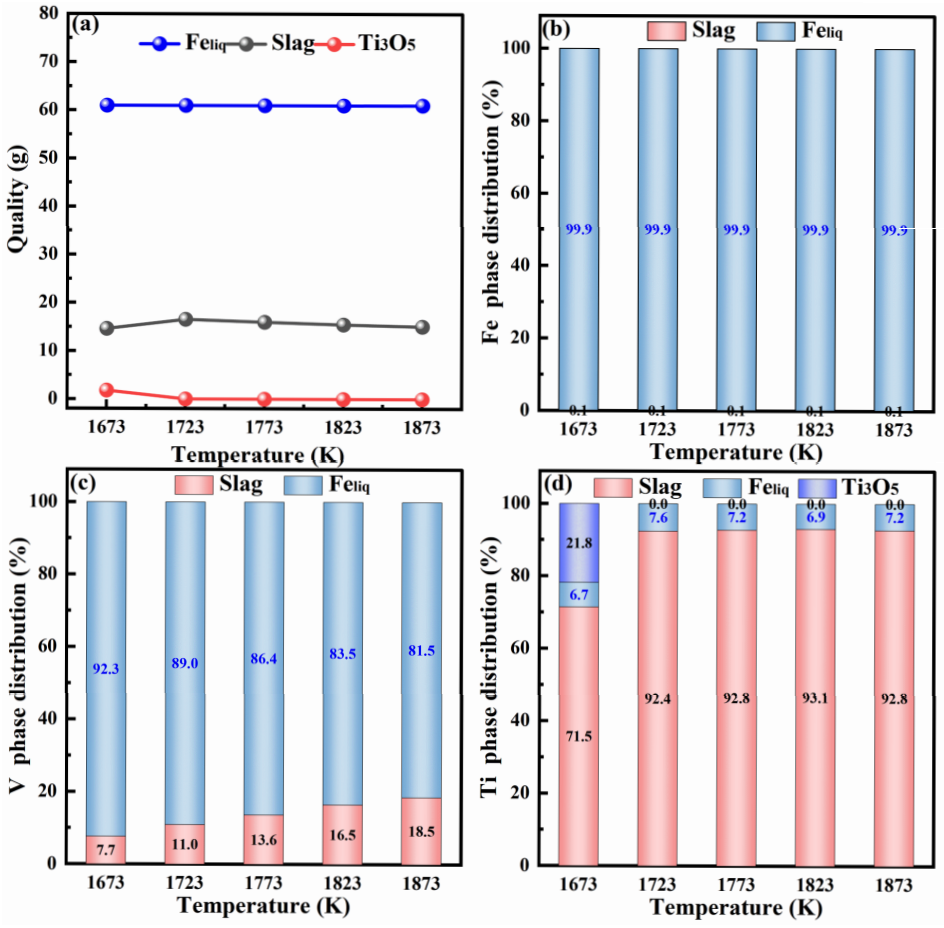


Figure 5. Calculated effect of temperature on the multicomponent complex thermodynamics during smelting with 6 wt% C addition: (**a**) phase distribution; (**b**) distribution behavior of Fe phases; (**c**) distribution behavior of V phases; (**d**) distribution behavior of Ti phases.

Table 8. Calculated Fe liquid phase composition at 6 wt% C addition/wt%.

Temperature/K	Fe	V	Ti	Si	C
1673	94.597	1.469	0.269	0.000	3.083
1723	94.568	1.417	0.620	0.000	2.738
1773	94.581	1.374	1.074	0.001	2.345
1823	94.580	1.329	1.495	0.002	1.993
1873	94.555	1.296	1.801	0.003	1.717

Table 9. Calculated slag composition with 6 wt% C addition (wt%).

Temperature/K	Fe	V	Ti	Ca	Si	Al	Mg	O
1673	0.48	0.51	25.84	0.73	8.47	15.86	5.61	42.50
1723	0.47	0.64	29.49	0.65	6.70	15.48	4.96	41.61
1773	0.42	0.83	30.65	0.67	5.19	16.03	5.13	41.08
1823	0.37	1.03	31.76	0.69	3.70	16.55	5.30	40.59
1873	0.33	1.19	32.54	0.71	2.55	17.01	5.45	40.23

Table 10. Calculated slag viscosity as a function of temperature with 6 wt% C addition.

Temperature/K	Viscosity/Pa·s
1673	0.323
1723	0.208
1773	0.152
1823	0.120
1873	0.100

When the C addition was increased to 8 wt%, a large amount of Ti was added into molten iron (Figure 6), indicating that over–reduction occurred and that the slag–metal separation during smelting consequently deteriorated. Considering the overall process performance, the optimal C addition was determined to be 6 wt%. These results suggest that the reduction sequence of valuable metals in pre–reduced V titanomagnetite follows the order: Fe_3O_4 > $(FeO)_{slag}$ > $(V_2O_5)_{slag}$ > $(Ti_2O_3)_{slag}$.

3.2. Slag Engineering for Carbothermal Smelting of Pre–Reduced VTM

To improve the slag viscosity and metal–slag separation while reducing the smelting temperature, CaO and MgO, which are the most widely used industrial additives, were introduced to examine their effects on slag physicochemical properties and valuable–metal recovery.

3.2.1. Thermodynamic Effect of CaO

Figure 7 and Tables 11–13 present the effects of CaO addition (0–4 wt%) at 1873 K on the distributions of Fe, V and Ti and on the elemental compositions of the Fe_{liq} and slag phases. The Fe distribution was barely influenced by CaO addition, and more than 99.80% of Fe remained in the Fe_{liq} phase throughout the tested range. In contrast, the transfer of V to the Fe_{liq} phase was continuously enhanced, with its distribution ratio increasing from 81.5% to 95.1% as the CaO addition increased from 0 to 4 wt%. In parallel, the V content in the Fe_{liq} phase increased from 1.296 wt% to 1.508 wt% (Table 12), indicating that CaO promoted the migration of V into the Fe_{liq} phase. Once the CaO dosage exceeded 3 wt%, the V recovery rose above 93.5% (Figure 7). In comparison, the Ti recovery exhibited minimal variation, remaining at approximately 91.1%, whereas the TiO_2 content in the slag remained above 24% (Table 12). Meanwhile, the slag viscosity decreased sharply from 0.100 to 0.048 Pa·s (Table 13), which facilitated the separation of the Fe liquid from the slag.

Overall, the CaO addition promoted valuable metal recovery during smelting, and the optimal dosage was determined to be 3 wt% based on economic factors.

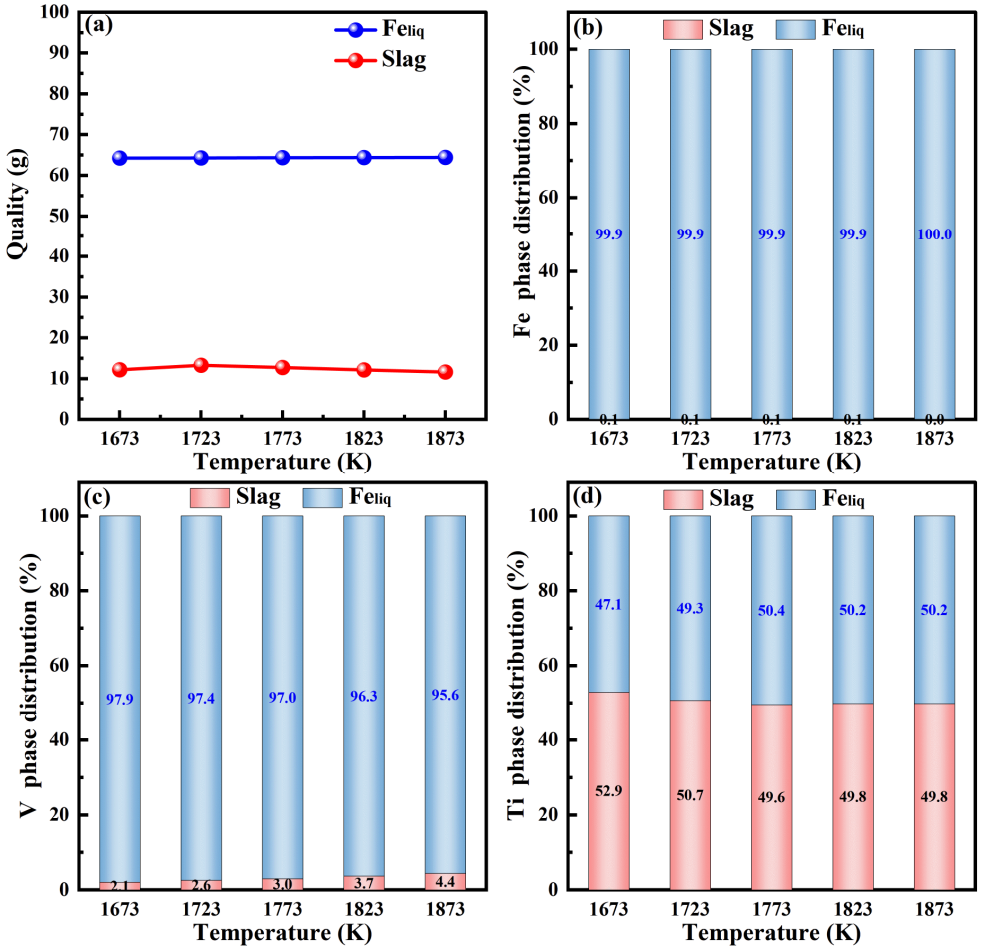


Figure 6. Calculated effect of temperature on the multicomponent complex thermodynamics during smelting with 8 wt% C addition: (**a**) phase distribution; (**b**) distribution behavior of Fe phases; (**c**) distribution behavior of V phases; (**d**) distribution behavior of Ti phases.

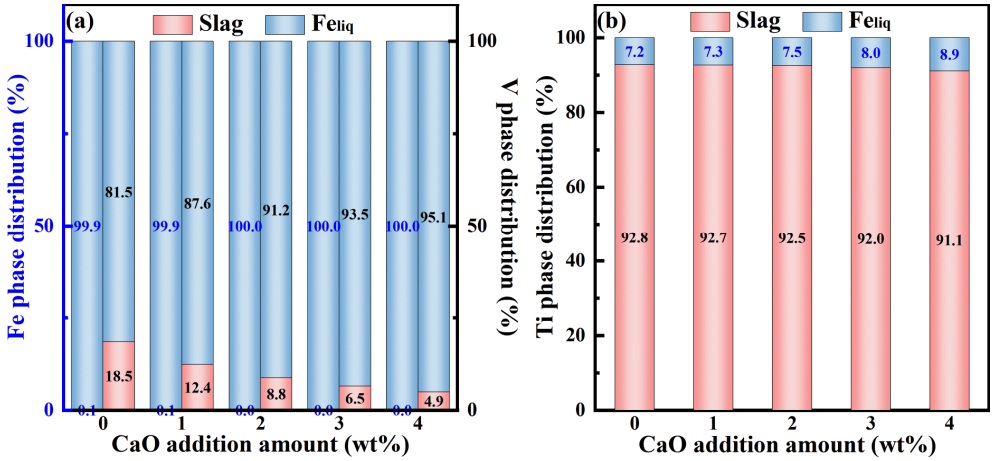


Figure 7. Calculated effect of temperature on the multicomponent complex thermodynamics during smelting: (**a**) distribution behaviors of Fe and V phases; (**b**) distribution behavior of Ti phases.

Table 11. Calculated composition of the liquid Fe phase as a function of CaO addition (%).

CaO/%	Fe	V	Ti	Ca	Si	C
0	94.555	1.296	0.627	0.000	1.801	1.717
1	94.515	1.392	0.631	0.000	1.608	1.849
2	94.473	1.448	0.647	0.000	1.427	2.000
3	94.417	1.484	0.693	0.000	1.236	2.165
4	94.351	1.508	0.764	0.000	1.038	2.334

Table 12. Calculated slag composition as a function of CaO addition (%).

CaO/%	Fe	V	Ti	Ca	Si	Al	Mg	O
0	0.33	1.19	32.54	0.71	2.55	17.01	5.45	40.23
1	0.21	0.74	30.21	5.07	3.09	15.80	5.06	39.81
2	0.15	0.49	28.10	8.84	3.52	14.72	4.72	39.46
3	0.11	0.34	26.14	12.12	3.92	13.78	4.41	39.19
4	0.08	0.24	24.33	15.00	4.30	12.94	4.14	38.97

Table 13. Calculated slag viscosity as a function of CaO addition at 1873 K (Pa·s).

CaO/%	Viscosity
0	0.100
1	0.076
2	0.062
3	0.054
4	0.048

3.2.2. Thermodynamic Effect of MgO

Figure 8 and Tables 14–16 present the effects of MgO addition (0–4 wt%) at 1873 K on the distributions of Fe, V and Ti, the elemental compositions of the Fe_{liq} and slag phases, and the crystalline phases of the slag at 1873 K. Similar to CaO, the increasing MgO addition improved V recovery. It increased from 81.5% to 90.2%, indicating that MgO also facilitated V transfer. However, the Ti partitioning to the Fe_{liq} phase also increased, rising from 7.2% to 10.7%, which was unfavorable for Ti recovery. Moreover, the slag viscosity decreased from 0.100 to 0.060 Pa·s as the MgO content increased (Table 16). These results indicate that MgO improved V recovery but weakened Ti recovery, and its effect on reducing slag viscosity was less pronounced than that of CaO. Therefore, when both recoveries and economic factors are considered, the MgO addition at 1673 K should be limited to below 3 wt%.

Table 14. Calculated composition of the liquid Fe phase as a function of MgO addition (%).

MgO/%	Fe	V	Ti	Ca	Si	Al	Mg	C
0	94.555	1.296	0.626	0.000	1.801	0.003	0.000	1.717
1	94.511	1.341	0.729	0.000	1.535	0.003	0.000	1.879
2	94.472	1.380	0.819	0.000	1.281	0.003	0.000	2.043
3	94.442	1.409	0.885	0.000	1.060	0.003	0.000	2.199
4	94.421	1.431	0.926	0.000	0.874	0.003	0.000	2.342

Table 15. Calculated slag composition as a function of MgO addition (%).

MgO	Fe	V	Ti	Ca	Si	Al	Mg	O
0	0.33	1.19	32.54	0.71	2.55	17.01	5.45	40.23
1	0.21	0.74	30.21	5.07	3.09	15.80	5.06	39.81
2	0.24	0.73	27.37	0.61	4.02	14.66	11.60	40.77
3	0.21	0.58	25.40	0.57	4.49	13.72	14.08	40.96
4	0.17	0.48	23.75	0.54	4.79	12.90	16.26	41.10

Table 16. Calculated slag viscosity as a function of MgO addition at 1873 K (Pa·s).

MgO/%	Viscosity
0	0.100
1	0.080
2	0.069
3	0.064
4	0.060

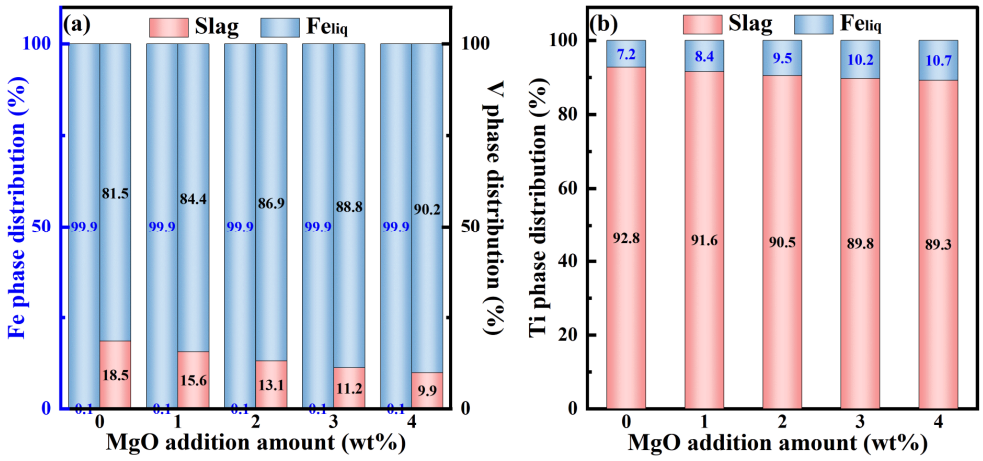


Figure 8. Calculated effect of temperature on the multicomponent complex thermodynamics during smelting, with 6 wt% C addition: (**a**) distribution behaviors of Fe and V phases; (**b**) distribution behavior of Ti phases.

4. Results and Discussion

4.1. Effect of MgO

A mixture of 2.5% semi–coke, 3–12 wt% MgO and pre–reduced VTM powder was thoroughly blended, pelletized in a crucible and held at 1873 K for 20 min to investigate the effect of MgO addition on the recovery of V, Fe and Ti from pre–reduced VTM. Under the condition of 3 wt% MgO addition, slag–alloy separation was not observed (Table 17), which differed markedly from the thermodynamic prediction in Section 3.2.2. XRD results (Figure 9) showed that the main phases in the slag were $(Mg,V)_xTi_{3-x}O_5$ (melting point: 2453 K), spinel ($MgAl_2O_4$, melting point: 2408 K), $(Ti,V)_2O_3$ (melting point: 2403 K) and Fe. Comparing Figures 1 and 9, the disappearance of $FeTiO_3$ and the appearance of $(Ti,V)_2O_3$ and $(Mg,V)_xTi_{3-x}O_5$ suggest that $FeTiO_3$ was first reduced by C to Fe, $V_xTi_{3-x}O_5$ and $(Ti,V)_2O_3$. In contrast, the added MgO entered these solid solutions and replaced the lattice V through a reaction with both phases. This process promoted the release of V and its conversion into chemically dissolved species, thereby facilitating subsequent reduction by C and transfer into the Fe–V alloy. However, because $MgAl_2O_4$, $(Ti,V)_2O_3$ and $(Mg,V)_xTi_{3-x}O_5$ possess high melting points, their melting at 1873 K is difficult, which

hinders the settling of the alloy, thereby suppressing the recovery of Fe and V. As shown in Figure 10, Fe existed in the form of a Fe–V alloy, whereas the slag phase contained almost no Fe. In addition, V was primarily concentrated in the $(Mg,V)_xTi_{3-x}O_5$ and $(Ti,V)_2O_3$ phases, with a content of 1.72 wt%, whereas the V content in the Fe–V alloy was only 0.57 wt%, corresponding to a predicted V recovery of only 30% under the assumption of slag–alloy separation.

Table 17. Effect of MgO addition on the recovery of V, Fe and Ti.

Semi–Coke/%	MgO/%	V/%	Fe/%	Ti/%	Note
2.5	3	/	/	/	
2.5	6	/	/	/	Poor slag–alloy separation
2.5	9	/	/	/	
2.5	12	/	/	/	

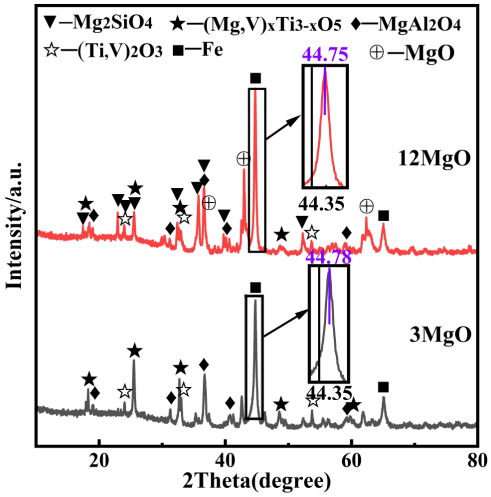


Figure 9. XRD pattern of slag with MgO additions.

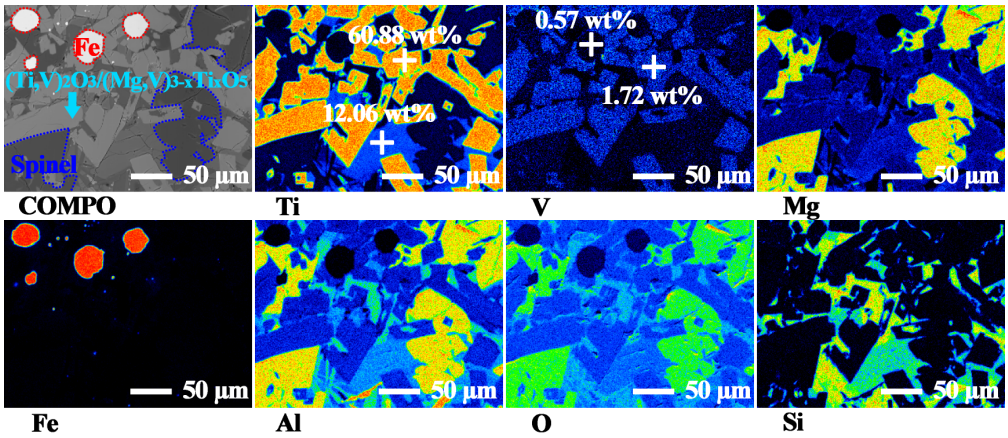


Figure 10. EPMA analysis of slag with 3 wt% MgO addition.

When the MgO addition was increased to 12 wt%, the slag–alloy separation became even worse. XRD analysis demonstrated that the intensity of Fe diffraction peaks in the slag increased, and the Fe diffraction peak shifted from 44.35° to 44.75°, which may be attributed to the entry of V with a smaller atomic radius into the Fe lattice. In addition, numerous Mg_2SiO_4 diffraction peaks appeared (Figure 9, 2163 K). The comparison of the electron microprobe analyses in Figures 10 and 11 showed that the size of the Fe–V alloy particles in the slag increased from 34 μm to more than 200 μm. This increase was attributed to the higher content of the amorphous phase, which reduced the slag viscosity and facilitated

the aggregation and growth of Fe–V alloy particles. Meanwhile, the V content in the Fe–V alloy increased from 0.57 wt% to 0.85 wt%. This result further indicates that MgO addition disrupted the crystal structure of $(Ti,V)_2O_3$ and released chemically dissolved V, which was subsequently reduced by C into the Fe–V alloy. However, excessive MgO also promoted the formation of Mg_2SiO_4 in the slag, thereby increasing slag viscosity and preventing the Fe–V alloy from settling. Therefore, the application of MgO as a modifier was not favorable for slag–alloy separation or V recovery.

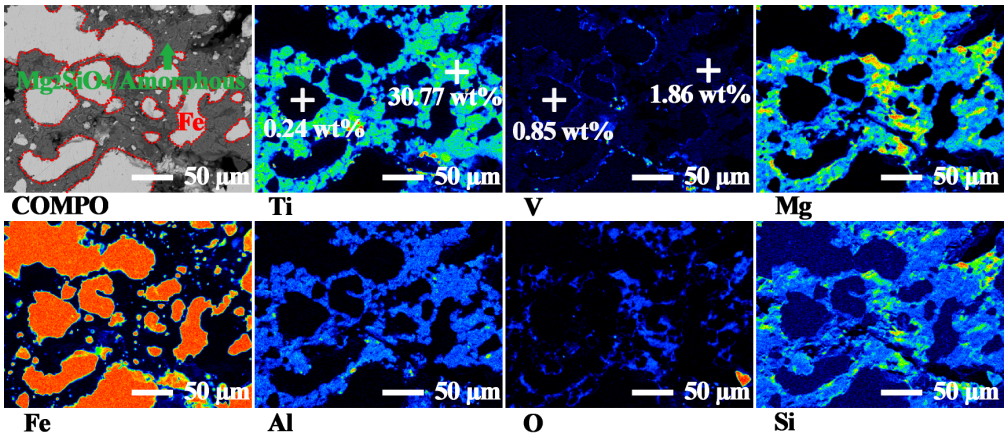


Figure 11. EPMA analysis of slag with 12 wt% MgO addition.

4.2. Effect of CaO

A mixture of 2.5% semi–coke, 3–15 wt% CaO and pre–reduced VTM powder was thoroughly blended and granulated in a crucible. The samples were then held at 1873 K for 20 min to simulate industrial production conditions, and the effect of CaO addition on the recovery of V, Fe and Ti from pre–reduced VTM was investigated. Unlike the case with 3 wt% MgO addition, outstanding slag–alloy separation was achieved with 3 wt% CaO addition. As shown in Table 18, the V content in the slag with 3 wt% CaO was 1.35 wt%, corresponding to a V recovery of 56.56%, while the recoveries of Fe and Ti reached 98.13% and 96.37%, respectively. These results indicate that CaO as a modifier is more favorable for V recovery and improves the slag–alloy separation condition. A comparison of Figures 9 and 12b indicates that the Fe diffraction peaks disappeared from the slag, whereas $CaAl_2Si_2O_8$ (calcium feldspar, melting point: 1826 K) appeared. This suggests that the liquid $CaAl_2Si_2O_8$ formed at 1873 K improved the slag mobility and rendered the slag–alloy separation possible. As shown in Figure 13, only a few small metallic Fe particles (<10 μm) remained in the slag, and the V contents in $(Ti,V)_2O_3$ and $CaAl_2Si_2O_8$ were 2.05 wt% and 0.28 wt%, respectively. In accordance with the thermodynamic stepwise reduction analysis, $FeTiO_3$ in the pre–reduced VTM was first reduced by C to Fe and $V_xTi_{3-x}O_5$, after which $V_xTi_{3-x}O_5$ was reduced by C to form $(Ti,V)_2O_3$. The added CaO then reacted with $(Ti,V)_2O_3$ to form $CaTiO_3$ and release $(V_xO_y)_{\text{chemically dissolved V}}$, which was subsequently reduced again by C and transferred to the Fe–V alloy (Figure S1).

Table 18. Effect of CaO on the V and Fe contents in the slag and the Ti content in Fe–V alloy.

CaO/wt%	V in Slag/wt%	Fe in Slag/wt%	Ti in Fe–V Alloy/wt%	V in Fe–V Alloy/wt%	Fe in Fe–V Alloy/wt%	Si in Fe–V Alloy/wt%
3	1.35	0.53	0.22	0.62	98.53	0.38
6	0.58	0.26	0.36	1.27	97.15	0.35
9	0.38	0.23	0.24	1.42	97.11	0.35
12	0.20	0.23	0.16	1.57	96.99	0.33
15	0.19	0.22	0.18	1.57	97.15	0.20

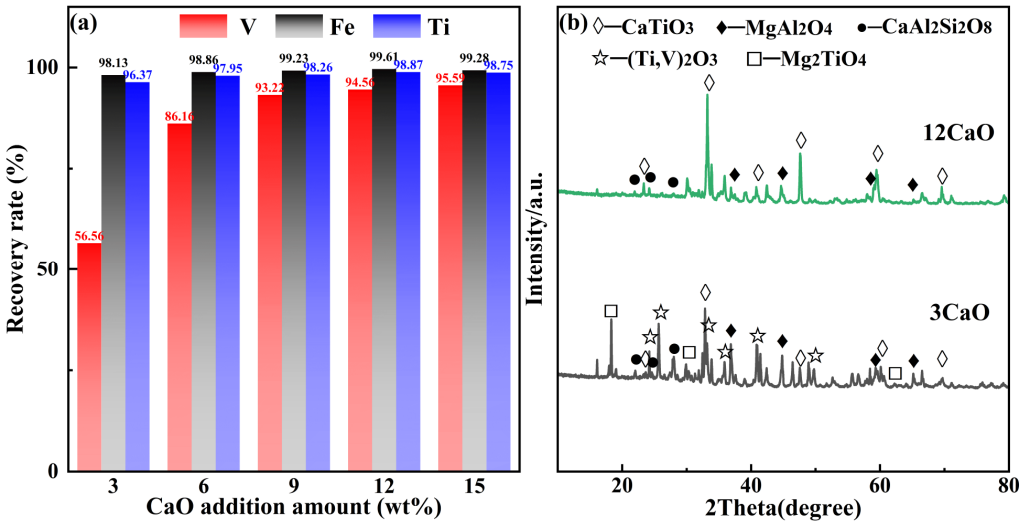


Figure 12. Effect of CaO addition on (**a**) the recovery of V, Fe and Ti; (**b**) XRD pattern of slag.

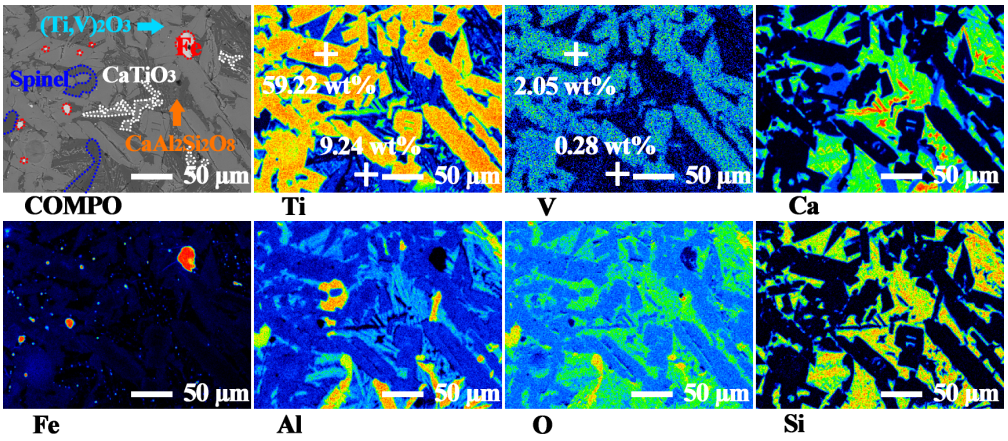


Figure 13. EPMA analysis of slag with 3 wt% CaO addition.

As the CaO addition gradually increased to 12 wt%, the V content in the slag decreased from 1.35 wt% to 0.20 wt% (Table 18). Meanwhile, the V recovery increased from 56.56% to 94.56% (Figure 12a). The recoveries of Fe and Ti remained above 98% and 96%, respectively. Similar to the role of MgO, this behavior indicates that CaO disrupts the crystal structure of $(Ti,V)_2O_3$ and promotes the release of chemically dissolved V for reaction with C. The XRD results in Figure 12b revealed that as the CaO addition increased to 12 wt%, the diffraction peaks of $(Ti,V)_2O_3$ disappeared. In contrast, the diffraction peaks of $CaTiO_3$ gradually appeared and intensified. At this stage, only $CaTiO_3$, spinel and calcium feldspar were detected. Figure 14 illustrates the disappearance of $(Ti,V)_2O_3$ and the formation of $CaTiO_3$. At this point, the bulk $(Ti,V)_2O_3$ phase (>150 μm) disappeared and was replaced by $CaTiO_3$, and the detected V signal was identified only in spinel and $CaTiO_3$ at 0.31 wt% and 0.43 wt%, respectively. This marked decrease in V content compared with the 3 wt% CaO condition was consistent with the reduction in slag V content from 1.35 wt% to 0.19 wt% with increasing CaO content (Table 18). These results confirmed that the CaO addition can promote V reduction and improve V recovery. Considering the recoveries of V, Fe and Ti with economic benefits, the optimal CaO addition was determined to be 12 wt%. Considering the MgO–based furnace lining, the simultaneous effect of CaO and MgO was further evaluated. With the addition of 0.5 wt% MgO on the basis of 12 wt% CaO, the slag contained 0.20 wt% V and 0.23 wt% Fe, and the Ti content in the alloy was 0.16 wt%. These results are almost identical to those obtained without MgO addition, indicating that

a minor amount of MgO from the lining has a negligible effect on the separation of Fe, V and Ti.

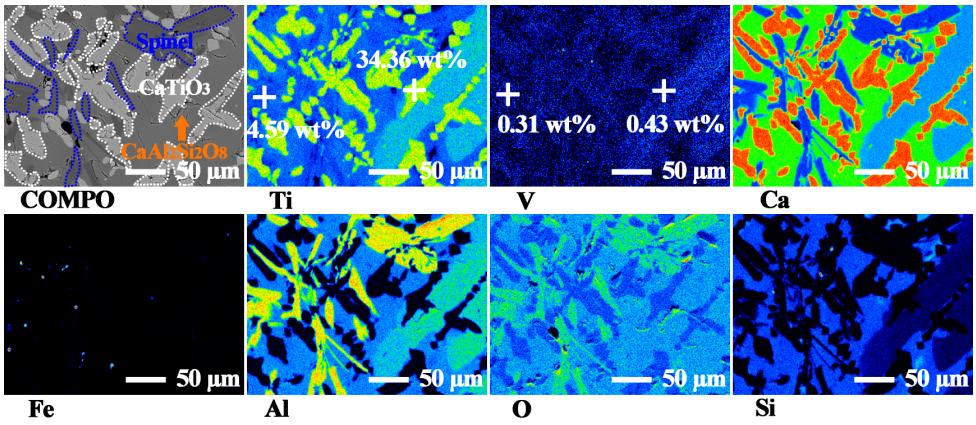


Figure 14. EPMA analysis of slag with 12 wt% CaO addition.

4.3. Migration and Transformation of Fe, V, and Ti During the Smelting Process

CaO and pre–reduced VTM powder was thoroughly blended, pelletized in a crucible and then rapidly water–quenched after holding at 1873 K for 2, 4, 5 and 6 min, respectively. The detailed results are presented in Table 19 and Figures 15–18. Owing to the brief holding time of 2 min, the slag entered the smelting zone but did not reach the target temperature of 1873 K, causing incomplete melting and no effective recovery of V, Fe or Ti (Table 19). The XRD pattern in Figure 15b showed that the slag at this stage consisted of $CaTiO_3$, $CaAl_2Si_2O_8$ and Fe. Because V doping shifted the Fe diffraction peak from the standard position of 44.35° to 44.76°, V remained undetectable by XRD at low concentrations. EPMA of the slag (Figure 16) indicated that the main phases were Fe, $CaTiO_3$ and $CaAl_2Si_2O_8$, with the V content in metallic Fe reaching 6.20 wt%. Combined with the reaction sequence of $FeTiO_3$, these observations indicated that the stepwise reduction of $FeTiO_3$ generated $(Ti,V)_2O_3$, which then reacted with the added CaO (Equation (1)) to form $CaTiO_3$ while simultaneously releasing chemically dissolved V. This dissolved V remained in the slag and contacted carbon, where it was reduced to metallic Fe (Equation (2)). This explains why the V content in $CaTiO_3$ was only 0.56 wt%, whereas 6.20 wt% V was identified in Fe.

$$(Ti,V)_2O_3 + CaO \rightarrow CaTiO_3 + (V_xO_y)_{\text{chemically dissolved V}} \quad (1)$$

$$(V_xO_y)_{\text{chemically dissolved V}} + C = [V]_{\text{Fe–V alloy}} + CO \quad (2)$$

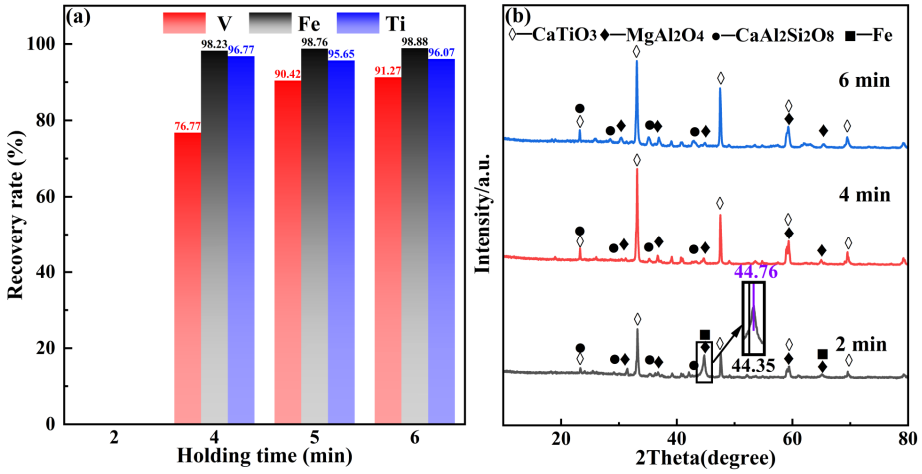


Figure 15. Effect of holding time on (**a**) the recovery of V, Fe and Ti; (**b**) XRD pattern of slag.

Table 19. Effect of holding time on the V and Fe contents in the slag and the Ti content in Fe–V alloy.

Holding Time/min	V in Slag/wt%	Fe in Slag/wt%	Ti in Fe–V Alloy/wt%
2	/	/	/
4	0.55	0.46	0.5
5	0.43	0.36	0.65
6	0.33	0.28	0.6

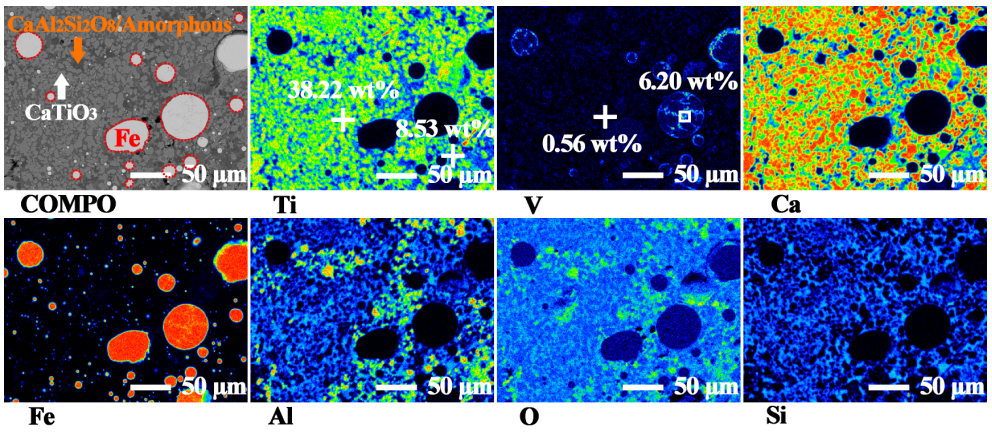


Figure 16. EPMA analysis of slag for holding 2 min.

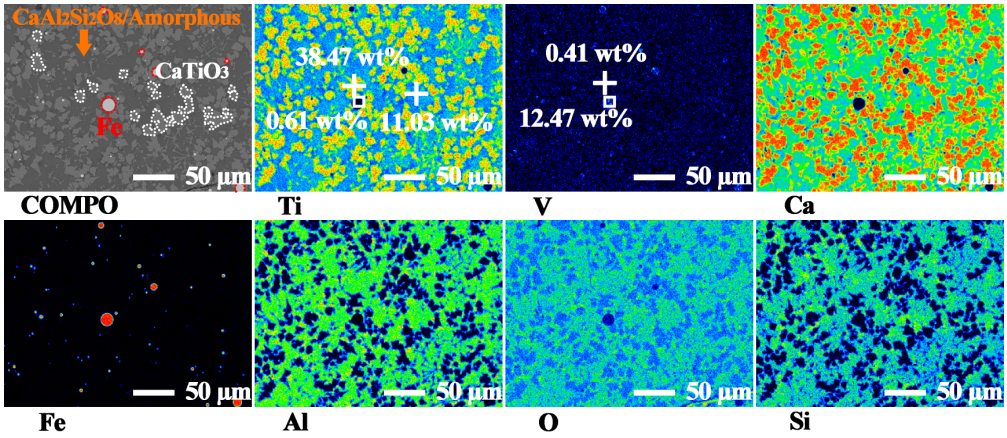


Figure 17. EPMA analysis of slag after holding for 4 min.

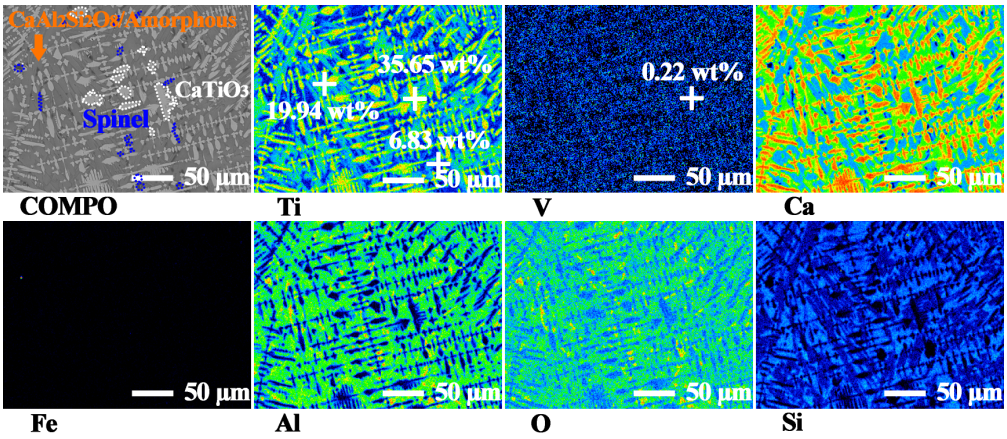


Figure 18. EPMA analysis of slag after holding for 6 min.

When the holding time was increased to 4 min, the slag began to melt and the slag–alloy separation started. As shown in Table 19, the V content in the slag decreased

to 0.55 wt%, and the corresponding V recovery increased to 76.77%. The XRD results showed that the Fe diffraction peaks disappeared, whereas the diffraction peaks of $CaTiO_3$, $CaAl_2Si_2O_8$ and spinel remained. This indicates that the slag contained almost no metallic Fe and confirms that Fe–V alloy sedimentation had been essentially completed. However, because a considerable amount of V remained, further recovery at this stage was mainly controlled by kinetics. Only a very small amount of metallic Fe (<12 μm) was present, and the main phases were $CaTiO_3$ and $CaAl_2Si_2O_8$, with V contents of only 12.47 wt% each. Combining Figures 15 and 17, the intensities of the diffraction peaks of $CaAl_2Si_2O_8$ were low, suggesting poor crystallinity. The comparison of Figures 16 and 17 indicates that the V content in Fe increased markedly from 6.20 wt% to 12.47 wt%, whereas the V content in $CaTiO_3$ decreased from 0.56 wt% to 0.41 wt%, further confirming the occurrence of Equation (1). When the holding time was extended to 6 min, the V content in the slag was further reduced to 0.23 wt% (Table 19), and the corresponding V recovery increased to 91.27%. The XRD pattern (Figure 15) showed no significant change in the diffraction peaks, and the main slag phases remained $CaTiO_3$ and $CaAl_2Si_2O_8$. Compared with Figures 17 and 18, the morphology of $CaTiO_3$ changed from granular to flocculent. This was because the slag had completely melted with prolonged holding for 6 min, whereas $CaTiO_3$ precipitated during water quenching owing to its higher melting point. At this stage, the Fe–V alloy in the slag had completely disappeared, and the V content in $CaTiO_3$ decreased from 0.41 wt% to 0.22 wt%. When the holding time was shorter than 6 min, $CaTiO_3$ in the slag was not fully melted because of kinetic limitations. Consequently, V in the $CaTiO_3$ lattice was difficult to reduce. The slag was completely melted only after holding for 6 min, allowing the chemically dissolved V and carbon to be fully contacted and the reduction reaction to proceed. It eliminated the kinetic barrier associated with low–temperature diffusion of chemically dissolved V to the slag–alloy interface, where it reacted with carbon, entered the Fe–V alloy and improved V recovery.

4.4. Effect of C

To examine the effect of semi–coke dosage on the recovery of V, Fe and Ti from pre–reduced VTM, the pre–reduced VTM powder was mixed with 12 wt% CaO and different amounts of semi–coke (1.5, 2.5, 3.5 and 4.5 wt%), followed by pelletizing and charging into a crucible. The mixtures were then maintained at 1873 K for 20 min. At a semi–coke addition of 1.5 wt%, the residual V and Fe contents in the slag were 1.63 wt% and 1.07 wt%, respectively, and the corresponding recoveries were only 34.44% for V and 96.13% for Fe (Table 20). Compared with the 1.5 wt% semi–coke condition, the V and Fe contents in the slag decreased to 0.20 wt% and 0.23 wt% for 2.5 wt% semi–coke additions. The XRD results (Figure 19) showed that the slag at this dosage was mainly composed of $CaTiO_3$, $CaAl_2Si_2O_8$ and spinel. The EPMA results for the slag with 1.5 wt% semi–coke (Figure 20) suggested that V was mainly concentrated in the Ti–V–Fe–Al–O phase and $CaTiO_3$, with contents of 4.09 wt% and 0.47 wt%, respectively. The Ti–V–Fe–Al–O phase was likely formed by segregation during slag cooling. Compared with Figure 14, the Fe content in $CaAl_2Si_2O_8$ increased to 1.54 wt%. These results indicate that chemically dissolved Fe was not fully reduced at this stage. Combined with the low V recovery of 34.44%, this suggests that chemically dissolved V was difficult to reduce effectively by C before the complete reduction of chemically dissolved Fe, which is consistent with the thermodynamic prediction. When the semi–coke addition was increased to 4.5 wt%, the residual V and Fe contents in the slag decreased to 0.30 wt% and 0.22 wt%, respectively, while the corresponding recoveries increased to 94.13% for V and 99.32% for Fe. Under this condition, chemically dissolved Fe was nearly absent from the slag, and the V recovery increased markedly from 34.44% to 94.13%. This further demonstrated that C preferentially

reduced the chemically dissolved Fe before reacting effectively with chemically dissolved V. Considering economic factors, the optimal smelting conditions for pre–reduced VTM were determined to be 1873 K with 2.5 wt% semi–coke and 12 wt% CaO.

Table 20. Effect of semi–coke on the V and Fe contents in the slag and the Ti content in Fe–V alloy.

Semi–Coke/wt%	V in Slag/wt%	Fe in Slag/wt%	Ti in Fe–V Alloy/wt%
1.5	1.63	1.07	0.21
2.5	0.20	0.23	0.16
3.5	0.27	0.21	0.18
4.5	0.30	0.22	0.17

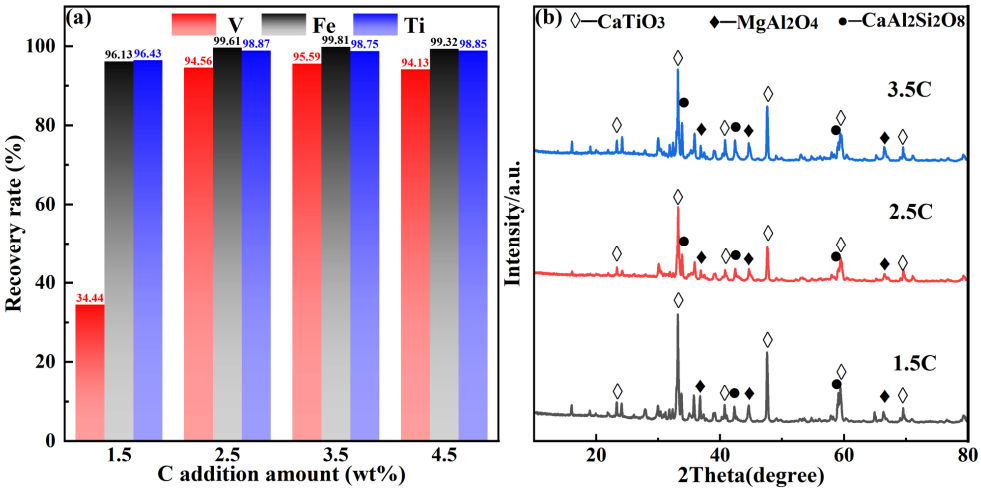


Figure 19. Effect of semi–coke on (**a**) the recovery of V, Fe and Ti; (**b**) XRD pattern of slag.

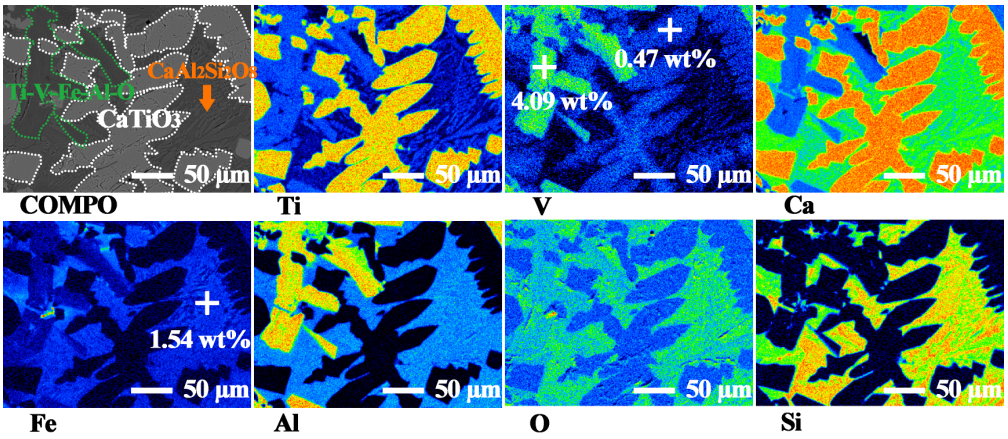


Figure 20. EPMA analysis of the slag with 1.5 wt% semi–coke addition.

5. Conclusions

The effects of MgO, CaO and semi–coke on the recovery of Fe, V and Ti were systematically investigated, and the migration and transformation pathways of V and Fe upon CaO addition were clarified.

1. With MgO addition, $FeTiO_3$ was first reduced by C to $V_xTi_{3-x}O_5$ and converted to $(Ti,V)_2O_3$. MgO subsequently entered the $(Ti,V)_2O_3$ structure and displaced V, thereby promoting the release of chemically dissolved V, which was then reduced by C and transferred to the Fe–V alloy. Meanwhile, MgO was found to react with slag at 1873 K to form large amounts of $MgAl_2O_4$ (melting point: 2408 K) and Mg_2SiO_4 (melting point: 2163 K),

markedly deteriorating slag fluidity. Slag–alloy separation was hindered, and the recoveries of V, Fe and Ti were consequently suppressed.

2. When CaO was used as the modifier, it reacted with $(Ti,V)_2O_3$ to form $CaTiO_3$ and release $(V_xO_y)_{\text{chemically dissolved V}}$. The chemically dissolved V was reduced to V and entered the $V_{\text{Fe–V alloy}}$. The reaction pathway was expressed as $FeTiO_3 \rightarrow V_xTi_{3-x}O_5$, Fe $\rightarrow (Ti,V)_2O_3 \rightarrow CaTiO_3$ and $(V_xO_y)_{\text{chemically dissolved V}} \rightarrow$ Fe–V alloy. During holding, CaO reacted with silicates to form $CaAl_2Si_2O_8$ (melting point: 1826 K), which reduced the slag viscosity, facilitated Fe–V alloy sedimentation and improved the recoveries of Fe and V.

3. Experiments conducted at 1873 K with 12 wt% CaO and different semi–coke dosages showed that the chemically dissolved Fe was reduced by C in preference to chemically dissolved V.

4. Under the optimal conditions of 1873 K, 20 min, 2.5 wt% semi–coke and 12 wt% CaO, the recoveries of V, Fe and Ti reached 94.56%, 99.61% and 98.87%, respectively. In comparison, the conventional processes achieved Fe and V recoveries of only 90% and 70%, respectively. These results indicate that the proposed process can effectively improve the recovery of Fe and V from pre–reduced VTM, thereby enhancing energy utilization efficiency and metal yield and supporting the industrial application of pre–reduced VTM.

Supplementary Materials: The following supporting information can be downloaded at https://www.mdpi.com/article/10.3390/ma19214582/s1. Figure S1: EPMA of alloy with 12 wt% CaO addition.

Author Contributions: C.Y.: Data curation, formal analysis, investigation, validation, writing—original draft; B.T.: Data curation, formal analysis, investigation, validation, writing—original draft; B.H.: Data curation, formal analysis, validation; F.Z.: Data curation, formal analysis, validation; Y.Y.: Conceptualization, funding acquisition, methodology, visualization, writing—original draft, writing—review & editing, supervision. P.W.: Methodology, project administration, supervision. All authors have read and agreed to the published version of the manuscript.

Funding: This work was supported in part by the Basic Research Fund of Zhongye Changtian International Engineering Co., Ltd. (2020JCYJ07), the National Natural Science Foundation of China (No. 52304423), and Yunnan Fundamental Research Projects (No. 202301BE070001–006).

Data Availability Statement: The original contributions presented in this study are included in the article/Supplementary Material. Further inquiries can be directed to the corresponding authors.

Conflicts of Interest: The authors Conglin Yao, Bing Hu, and Fuqiang Zheng were employed by Zhongye Changtian International Engineering Co., Ltd. The authors declare that this study received funding from Zhongye Changtian International Engineering Co., Ltd. The funding sponsors had the following involvement with the study: data curation, formal analysis, investigation, validation, and writing—original draft. The remaining authors declare no conflicts of interest.

References

1. Nkosi, S.; Goso, X.C.; Mokone, T.; Petersen, J.; Bungane, T. Discounted Cash Flow Analysis of a Process for Vanadium Extraction from Titaniferous Slag. *Minerals* **2026**, *16*, 378. [CrossRef]
2. Sadangi, J.K.; Pati, S.; Biswal, S.K. Development of Suitable Process for Beneficiation of Low–Grade Vanadium Titanomagnetite Ore to Enhance the Vanadium, Titanium, and Iron Content. *Trans. Indian Inst. Met.* **2026**, *79*, 41. [CrossRef]
3. Wang, S.; Li, G.; Guo, Y.; Chen, F.; Jing, J.; Zhang, J.; Yang, L.; Qiu, G. Effects of MnO on the smelting process of vanadium titanomagnetite pre–reduced pellets in an electric furnace. *J. Mater. Res. Technol.* **2022**, *20*, 2262–2270. [CrossRef]
4. Kim, R.; Chung, K.W.; Lee, S.; Kim, M.; Lee, J.; Nam, C.–.W.; Yoon, H.–.S.; Kim, C.–.J. Comprehensive Mineralogical and Metallurgical Interpretation on the Recovery of Vanadium from a Korean Vanadium–Bearing Titaniferous Magnetite Ore via Pyro–Hydrometallurgical Consecutive Process. *Min. Metall. Explor.* **2025**, *42*, 4103–4114. [CrossRef]

5. Yan, Z.; Zhang, Y.; Zheng, S.; Zhang, Y.; Sun, P.; Song, Z.; Safdar, F.; Qi, T. Preparation of titanium mineral from vanadium titanomagnetite concentrates by hydrogen reduction and acid leaching. *Trans. Nonferrous Met. Soc. China* **2022**, *32*, 3099–3109. [CrossRef]
6. Trinh, H.B.; Kim, S.; Lee, J.; Oh, S. Efficient Recovery of Vanadium and Titanium from Domestic Titanomagnetite Concentrate Using Molten Salt Roasting and Water Leaching. *Materials* **2023**, *16*, 6918. [CrossRef]
7. Han, Y.; Dou, Z.; Yang, Z.; Xie, W.; Zhang, T. Process mechanism research on direct vortex melting reduction of vanadium–titanium magnetite. *J. Iron Steel Res. Int.* **2025**, *32*, 536–549. [CrossRef]
8. Oke, E.A.; Potgieter, J.H.; Nkhoesa, D.; Dyk, L.D.V. Vanadium, Titanium, and Iron Extraction from Titanomagnetite Ore by Salt Roasting and 21st–Century Solvents. *Separations* **2025**, *12*, 285. [CrossRef]
9. Wang, Z.; Liu, W.; Rohani, S.; Xin, Y.; Chen, L.; Qin, Z.; Luo, D. Hydrogen–based reduction of vanadium–titanium magnetite: A review. *Miner. Eng.* **2025**, *232*, 109490. [CrossRef]
10. Zhu, F.; Ma, Z.; Gao, G.; Qiu, K.; Peng, W. Process Mineralogy of Vanadium Titanomagnetite Ore in Panzhihua, China. *Separations* **2023**, *10*, 147. [CrossRef]
11. Zhang, S.; Wang, Z.; Hu, P.; Rao, J.; Zong, Y.; Pang, J. Influence of composition and temperature on distribution behavior of V, Ti and Si in HIsmelt. *Trans. Nonferrous Met. Soc. China* **2023**, *33*, 3835–3846. [CrossRef]
12. Han, J.; Zhang, J.; Zhang, J.; Chen, X.; Zhang, L.; Tu, G. Recovery of Fe, V and Ti in modified Ti–bearing blast furnace slag. *Trans. Nonferrous Met. Soc. China* **2022**, *32*, 333–344. [CrossRef]
13. Fu, W.; Wen, Y.; Xie, H. Development of Intensified Technologies of Vanadium–Bearing Titanomagnetite Smelting. *J. Iron Steel Res. Int.* **2011**, *18*, 7–10. [CrossRef]
14. Sui, Y.; Guo, Y.; Travyanov, A.Y.; Jiang, T.; Chen, F.; Qiu, G. Reduction roasting–magnetic separation of vanadium tailings in presence of sodium sulfate and its mechanisms. *Rare Met.* **2016**, *35*, 954–960. [CrossRef]
15. Li, H.; Han, Y.; Jin, J.; Gao, P.; Zhou, Z. Process mineralogy approach to optimize curing–leaching in vanadium–bearing stone coal processing plants. *Int. J. Min. Sci. Technol.* **2023**, *33*, 123–131. [CrossRef]
16. Yi, Y.; Sun, H.; You, J.; Zhang, J.; Cai, Y.; Zhang, X.; Luo, J.; Qiu, G. Vanadium recovery from Na_2SO_4–added V–Ti magnetite concentrate via grate–kiln process. *Trans. Nonferrous Met. Soc. China* **2022**, *32*, 2019–2032. [CrossRef]
17. Shi, Y.; Zhu, D.; Pan, J.; Guo, Z.; Lu, S.; Xue, Y. Investigation into the coal–based direct reduction behaviors of various vanadium titanomagnetite pellets. *J. Mater. Res. Technol.* **2022**, *19*, 243–262. [CrossRef]
18. Luo, Y.; Che, X.; Cui, X.; Zheng, Q.; Wang, L. Selective leaching of vanadium from V–Ti magnetite concentrates by pellet calcification roasting–H_2SO_4 leaching process. *Int. J. Min. Sci. Technol.* **2021**, *31*, 507–513. [CrossRef]
19. Zhang, Y.; Wang, L.; Chen, D.; Wang, W.; Liu, Y.; Zhao, H.; Qi, T. A method for recovery of iron, titanium, and vanadium from vanadium–bearing titanomagnetite. *Int. J. Miner. Metall. Mater.* **2018**, *25*, 131–144. [CrossRef]
20. Chen, L.; Zhen, Y.; Zhang, G.; Chen, D.; Wang, L.; Zhao, H.; Meng, F.; Qi, T. Carbothermic reduction of vanadium titanomagnetite with the assistance of sodium carbonate. *Int. J. Miner. Metall. Mater.* **2022**, *29*, 239–247. [CrossRef]
21. Yang, S.; Liu, S.; Guo, S.; Zhang, T.; Li, J. Fusion Separation of Vanadium–Titanium Magnetite and Enrichment Test of Ti Element in Slag. *Materials* **2022**, *15*, 6795. [CrossRef]
22. Long, Z.; Bing, H.; Zhu, H.; Wu, Y. Soil covering measure mitigates vanadium loss during short–term simulated rainfall in the vanadium titano–magnetite tailings reservoir. *J. Environ. Manag.* **2023**, *330*, 117201. [CrossRef]
23. Gan, C.; Cui, S.; Wu, Z.; Yang, J. Multiple heavy metal distribution and microbial community characteristics of vanadium–titanium magnetite tailing profiles under different management modes. *J. Hazard. Mater.* **2022**, *429*, 128032. [CrossRef]
24. Wang, H.; Ye, C.; Ge, R.; Teng, B.; Zhu, J.; Wang, C. Addressing the challenges of per–and polyfluoroalkyl substances (PFAS) contamination: Overview of contamination status, treatment technologies and prospects. *Process Saf. Environ. Prot.* **2026**, *207*, 108370. [CrossRef]
25. Cheng, G.J.; Gao, Z.X.; Yang, H.; Xue, X.X. Effect ofcalcium oxide on the crushing strength, reduction, and smelting performance of high–chromium vanadium–titanium magnetite pellets. *Metals* **2017**, *7*, 181. [CrossRef]
26. Wang, S.; Guo, Y.; Zheng, F.; Chen, F.; Yang, L.; Chen, M.; Zhao, B.; Jiang, T. Optimization of Basicity of High Ti Slag for Efficient Smelting of Vanadium Titanomagnetite Metallized Pellets. *Metall. Mater. Trans. B* **2020**, *51*, 945–952. [CrossRef]
27. Chen, C.; Sun, T.; Kou, J.; Wang, X.; Zhao, Y. Feasibility study on preparation of magnesium titanate in carbonthermic reduction of vanadium titanomagnetite concentrates. *Physicochem. Probl. Miner. Process.* **2019**, *55*, 417–425. [CrossRef]
28. Gao, Z.X.; Cheng, G.J.; Xue, X.X.; Yang, H.; Duan, P.N. Property investigations of low–grade vanadium–titanium magnetite pellets with different MgO contents. *Steel Res. Int.* **2018**, *89*, 1700543. [CrossRef]
29. Chen, C.; Sun, T.; Wang, X.; Hu, T. Effects of MgO on the Reduction of Vanadium Titanomagnetite Concentrates with Char. *JOM* **2017**, *69*, 1759–1766. [CrossRef]
30. *GB/T 14506.32–2019*; Methods for Chemical Analysis of Silicate Rocks–Part 32: Determination of Aluminum Oxide Content. Standards Press of China: Beijing, China, 2019.

31. *GB/T 14353.1–2010*; Methods for Chemical Analysis of Copper Ores, Lead Ores and Zinc Ores–Part 1: Determination of Copper Content. Standards Press of China: Beijing, China, 2010.
32. *YB/T 4177.2–2025*; Determination of Multi-Element Content in Slag—Inductively Coupled Plasma Optical Emission Spectrometry. Ministry of Industry and Information Technology: Beijing, China, 2025.

Disclaimer/Publisher's Note: The statements, opinions and data contained in all publications are solely those of the individual author(s) and contributor(s) and not of MDPI and/or the editor(s). MDPI and/or the editor(s) disclaim responsibility for any injury to people or property resulting from any ideas, methods, instructions or products referred to in the content.